

1 F18-PSMA Cerenkov luminescence and flexible autoradiography Imaging in a
2 prostate cancer mouse model and first results of a radical prostatectomy feasibility
3 study in men
4
5
6

7 Fragoso Costa Pedro^{1, 2*}, Püllen L^{2, 3*}, Kesch C^{2, 3}, Krafft U^{2, 3}, Tschirdewahn S^{2, 3}, Moraitis A^{1, 2},
8 Radtke JP^{2, 3}, Ting S⁴, Nader M^{1, 2}, Wosniack J^{1, 2}, Kersting D^{1, 2}, Lückcrath K^{1, 2}, Herrmann K^{1, 2},
9 Fendler WP^{1, 2}, Hadaschik BA^{2, 3}, Darr Christopher^{2, 3}

10
11 * contributed equally
12

13 **Running title:**

14 Translation of ¹⁸F-PSMA CLI and FAR-CLI
15

16
17 Words: 5067/
18

19 1 - Department of Nuclear Medicine, University Hospital Essen, Essen, Germany
20 2 - German Cancer Consortium (DKTK)-University Hospital Essen, Essen, Germany
21 3 - Department of Urology, University Hospital Essen, Essen, Germany
22 4 - Institute of Pathology, University Duisburg-Essen, Essen, Germany
23
24
25
26
27

28 **Corresponding author:**

29 Dr. med. Christopher Darr
30 Department of Urology
31 University Hospital Essen
32 Hufelandstr. 55
33 45147 Essen, Germany
34 E-Mail: Christopher.Darr@uk-essen.de
35 Phone.: 0049 201-723/85633
36 Fax.: 0049 201-723/3151
37

1 **Abstract**

2 Objective

3 Intraoperative identification of positive resection margins (PRM) in high-risk prostate cancer (PC)
4 needs improvement. Cerenkov Luminescence Imaging (CLI) with ⁶⁸Ga-PSMA-11 is promising,
5 however limited by low residual activity and artificial signals. Here, we aim to assess the value of
6 CLI and flexible autoradiography (FAR) with ¹⁸F-PSMA-1007.

7
8 Methods

9 Mice bearing subcutaneous PSMA-avid RM1-PGLS tumors were administered ¹⁸F-PSMA-1007
10 and PET/CT was performed. After sacrifice, organs were excised and measured signals in CLI
11 and FAR-CLI were correlated with tracer activity concentrations (AC) obtained from PET/CT. For
12 clinical assessment, seven high-risk PC patients underwent radical prostatectomy (RP)
13 immediately after preoperative ¹⁸F-PSMA-PET/CT. Contrast-to-noise ratios (CNR) were
14 calculated for both imaging modalities in intact specimen and after incision above the index lesion.

15
16 Results

17 In the heterotopic in vivo mouse model (n=5), CLI did not detect any lesion. FAR-CLI detected a
18 distinct signal in all mice with a lowest AC of 7.25 kBq/ml (CNR: 5.48). After incision above the
19 index lesion of the prostate specimen, no increased signal was observed at the cancer area in
20 CLI. In contrast, using FAR-CLI a signal was detectable in 6 of 7 patients. AC in the missed index
21 lesion was 1.85 kBq/ml, resulting in a detection limit of at least 2.06 kBq/ml. Histopathology
22 demonstrated 2 PRM, none of which were predicted by CLI or FAR-CLI.

23
24 Conclusion

25 ¹⁸F-PSMA FAR-CLI was superior to CLI in terms of tracer-related signal detectability. Visualization
26 of PC was possible in RP down to 2.06 kBq/ml. However, the detection of PRM was limited. Direct
27 anatomical correlation of FAR-CLI is challenging due to the scintillator overlay.

28
29 **Key words:** Flexible Autoradiography, Cerenkov Luminescence Imaging, Prostate cancer, margin
30 assessment

1 Introduction

2 Negative resection margins are a key-component of tumor surgery in curatively intended
3 interventions. Radical prostatectomy (RP) is one of the treatment options along with radiotherapy
4 in men with localized or locally advanced prostate cancer (PC)(1). Positive resection margins
5 (PRM) occur in 11-38% of patients undergoing RP, resulting in a higher risk of recurrence and
6 disease-related mortality by a factor of three (2,3).

7 Preoperative magnetic resonance imaging (MRI) and nomograms have become widely
8 used for local staging of the disease and prediction of extracapsular extension. Recently, PSMA-
9 PET/CT was also included in the primary diagnosis of high-risk prostate cancer in the guidelines
10 (1). Besides this, the use of intraoperative frozen section analysis (IFS) reduces PRM to 15% for
11 all stages (4-6). Consequently, there is a wish to accurately detect malignant areas in real-time
12 during RP to ensure complete removal of PC.

13 Currently, there are several newly implemented technologies for margin assessment with
14 promising results, but some of them lack large clinical studies to be subsequently used in clinical
15 routine. Intraoperative conditions affecting the signal, long imaging times and comparison with
16 histopathology are the main challenges (7,8).

17 Previously developed gamma counters are well established with single photon emitting
18 radionuclides (9). Maurer et al demonstrated reliable identification of small and/or atypically
19 localized lesions for ^{99m}Tc-PSMA-guided surgery. The procedure has proven to be valuable for
20 the successful intraoperative detection and removal of metastatic lesions in PC patients scheduled
21 for salvage surgery (10-13).

22 The same technique has been successfully applied to beta-plus emitters, giving way to
23 potentially every radioligand used in diagnostic PET/CT to be used in radioguided surgery (14).
24 Other ex vivo imaging techniques, such as the use of a micro-PET/CT for three-dimensional
25 analysis of lesions, which could provide volumetric information about the removed specimens,
26 currently require further study-based investigation (15). In patients with biochemical recurrence,
27 PSMA-PET/CT demonstrates high accuracy, allowing surgical resection to be pursued for single
28 lymph node metastases. Recently, the introduction of a so-called drop-in γ -probe has allowed for
29 PSMA-guided surgery during minimally invasive robot-assisted surgery. Intraoperatively, γ -probes
30 not only facilitate intraoperative in vivo guidance but also enable ex vivo measurements to confirm
31 successful resection of these metastatic PC lesions, with a specificity of more than 95% for ^{99m}Tc-
32 PSMA-I&S(11).

33 Cerenkov Luminescence Imaging (CLI) is based on the detection of photons produced in
34 a dielectric medium, when the medium interacts with β -particles traveling at a speed greater than

1 the velocity of light. Cerenkov luminescence predominantly comprises ultraviolet and blue light,
2 that is highly susceptible to attenuation in biological tissue, therefore, limiting CLI to the detection
3 of signals emitted in superficial tissue layers (16,17). In the context of RP, the detected signals
4 can accordingly be indicative of a PRM (13,14).

5 Feasibility and safety of ^{68}Ga -PSMA-CLI has recently been demonstrated in RP. However,
6 it must be noted here that so far only feasibility studies are described and larger multicenter
7 randomized trials are pending. In addition, clinical application without intraoperative tracer
8 injection is challenged by the short half-life of ^{68}Ga and the time required for prostate removal. (18-
9 20). ^{18}F -PSMA-CLI would easily overcome this restriction with respect to the half-life. However,
10 one limitation for ^{18}F may arise from having a theoretically 26-fold lower Cherenkov light yield
11 compared to ^{68}Ga , which is caused by the lower β^+ -energy (21).

12 An alternative way of generating photons that can be detected by the same imaging system
13 as in CLI may be introduced by adding a scintillator between the specimen and the detectors. In
14 this novel approach, called flexible autoradiography (FAR), scintillations are produced by a
15 micrometers-thick flexible scintillating film draped over an excised specimen (Supplementary
16 Figure 1). The physical principle differs from CLI in that the high-energy β -particles from the
17 radiotracer interact with the scintillator, which, subsequently, produces photons in the visible light
18 spectrum. Since the Cerenkov photons are also detected, this is referred to as FAR-CLI. The main
19 advantage of a flexible scintillation film compared to conventional rigid autoradiography
20 techniques is that it conforms to the shape of the excised specimen. By maximizing the contact
21 area, sectioning of the tissue can be eliminated and increased signal intensity can be achieved.
22 The thinness of flexible scintillator makes it insensitive to the ^{18}F 511 keV γ -photons (22,23). FAR-
23 CLI in an in-vitro preclinical application increased the signal for ^{18}F by a factor of 11, allowing for
24 further development of ^{18}F tracers also in the context of intraoperative imaging (24). The behavior
25 of ^{18}F -PSMA-CLI and ^{18}F -PSMA-FAR-CLI in human perfused tissue undergoing RP is unknown.

26 The primary objective of the study is to investigate the feasibility of both modalities in RP,
27 with examination of the minimum detectable activity level as a secondary objective.

28 In this study we first investigated the applicability of both imaging modalities – ^{18}F -PSMA-
29 CLI and ^{18}F -PSMA-FAR-CLI - in a mouse model, that processes similar optical characteristics to
30 those of prostate tissue, and then translated findings to radical prostatectomy. To our knowledge
31 we are the first to perform CLI and FAR-CLI using ^{18}F -PSMA in PC patients.

32

1 **Material and methods**

2 To investigate the imaging behavior and minimum detectable activity concentration of ¹⁸F-
3 PSMA-1007 in CLI and FAR-CLI, a two-step approach was conducted (Figure 1). First, multi-
4 modal PET/CT (β-Cube / X-Cube, Molecubes, Belgium), as well as CLI and FAR-CLI imaging with
5 the LightPath® system (Lightpoint Medical Ltd., Chesham, UK) were performed in mice bearing
6 subcutaneous PSMA-avid RM1-PGLS tumors (25). Subsequently, the findings were transferred
7 and evaluated in RP. Studies were formally approved by the North Rhine-Westphalia State
8 Agency for Nature, Environment and Consumer (LANUV; Z.81-02.04.2018.A090) and the local
9 Ethical Committee of the University of Duisburg-Essen and the ethics committee (19-8749-BO).
10 Additionally, a dilution series with ¹⁸F-PSMA was prepared and used to measure CLI and FAR-
11 CLI in Eppendorf-tubes. This was performed to assess the device's performance in respect to
12 linearity and minimum detectable activity concentration in the absence of tissue.

13

14 Preclinical-Setup: Mouse model

15 RM1-PGLS cells were cultured in Rosewell Park Memorial Institute 1640 medium/10%
16 fetal bovine serum at 37°C and 5% CO₂. Contamination with *Mycoplasma* was excluded using the
17 Venor GeM *Mycoplasma* detection kit (Sigma Aldrich).

18 Male C57BL/6 mice (5-12 weeks-old, x -y g, Charles River) were bred and housed under
19 pathogen-free conditions, with food and water *ad libitum* and a 12/12 hour light-dark cycle. Eight
20 days before intraperitoneal injection of 2.61 MBq (range: 2.02 – 3.06 MBq) ¹⁸F-PSMA-1007, RM1-
21 PGLS (0.1 x 10⁶ cells in Matrigel:PBS = 1:1) were injected subcutaneously into the shoulder region
22 (n=5 mice). MicroPET/CT was performed at 2 hours post injection (p.i.) and reconstructed ACs
23 were used to correlate the CLI and FAR-CLI signals. Immediately after microPET/CT, mice were
24 sacrificed for CLI and FAR-CLI. The first CLI/FAR-CLI imaging set-up included the whole mouse
25 in order to visualize both kidneys and the shoulder region in the LightPath® system. The kidneys
26 and tumor tissue were then excised and re-examined with the LightPath system. The main
27 rationale for using mouse specimens was that, in principle, they should have similar optical
28 characteristics as those of the prostate, and with this provide a more valid surrogate for sensitivity
29 than Eppendorf tubes, for example (26).

30

31 Clinical-Setup: Radical prostatectomy

32 Patients with histologically confirmed PC without metastases on conventional staging were
33 scheduled for radical prostatectomy (RP). On the day of surgery, ¹⁸F-PSMA-1007 was injected
34 intravenously for routine PSMA-PET staging prior to surgery (27). Approximately 60 minutes post-

1 injection, PET/CT was performed and assessed by dedicated specialists in Nuclear Medicine. In
2 case of high-volume metastatic disease on PET/CT, same-day surgery would have been
3 cancelled. Following PET/CT, RP was performed by one experienced surgeon ahead of extended
4 pelvic lymph node dissection to minimize signal intensity reduction from radiotracer decay in the
5 time between ^{18}F -PSMA injection and CLI/FAR-CLI imaging. After retrieval of the prostate, the
6 prostate was rinsed twice to clear any potential radioactive contamination from blood or urine
7 followed by imaging of the entire specimen. A total of two or three images were necessary to
8 capture all sides of the prostate. MRI-guided incision above the index lesion was then performed
9 followed by imaging (CLI and FAR-CLI) of the lesion. This allowed direct examination of the tumor
10 tissue with assessment of the present luminescence, corresponding to a PRM. Upon
11 investigational imaging completion, the prostatectomy specimen was sent for postoperative
12 histopathological analysis. We recently demonstrated that a single injection of ^{68}Ga -PSMA as part
13 of the PET/CT/CLI procedure is associated with acceptable occupational exposure (28).
14 According to the model, the use of ^{18}F -PSMA would increase occupational exposure
15 comparatively to ^{68}Ga -PSMA, allowing for 117 procedures until the lower occupational yearly limit
16 of 6 mSv is reached. Continuous monitoring of the exposed personnel is carried out in accordance
17 with the legal requirements. Due to the design of this feasibility study, the surgical course remained
18 unaffected by the intraoperative imaging results, and no further tissue was resected if positive
19 margins were suspected.

20

21 Imaging and image analysis

22 The LightPath® System, an in vitro diagnostic device, was used to visualise the location
23 of ^{18}F -PSMA for CLI and FAR-CLI. This system is further described by Ciarrocchi et al.(29). Both
24 a luminescence image and a gray-scaled image of the specimen were captured through the
25 system. Both CLI and FAR-CLI were acquired standardized with an acquisition time of 300
26 seconds, 8x8 binning and no optical filter (29). Of note, image acquisition must be performed in a
27 light-tight chamber. The 12- μm -thick flexible scintillating film (Lightpoint Medical Ltd., Chesham,
28 UK) used in FAR-CLI, consisted of a multilayer sandwich construction as follows: 3 μm of mylar,
29 6 μm of P43 scintillating phosphor and 3 μm of mylar (22).

30 Background signals and elevated signals of both imaging modalities were subsequently
31 analysed using PMOD (PMOD Version 3.204, PMOD Technologies LLC). Measurements of the
32 mean radiance (photons/s/cm²/sr) were performed in regions of interest (ROIs) with a 50%-
33 threshold. 2 dimensional ROIs were selected in areas showing increased signal intensity (tumor)
34 or no increased signal (tissue background) to calculate contrast-to-noise ratios (CNRs):

1
2
3
4
5
6
7
8
9
10
11
12
13
14

$$CNR = \frac{Tumor_{avg} - Bkg_{avg}}{Bkg_{SD}}$$

In the absence of increased signal, the corresponding MRI-informed target lesion was contoured. In terms of detectability, foci were considered sufficiently visible with a CNR equal or greater than 5, a condition also referred to as the rose-criterion (30).

Statistical analysis

Numerical variables were summarized with median values and interquartile ranges (IQR), categorical variables with proportions (%). To compare medians of non-parametric data, the Mann-Whitney-U test was used for 2 groups. Spearman's correlation coefficient was used for correlation, significance set at p<0.05. The CLI CNR values were plotted as a function of the measured PET mean AC (decay corrected to the time of CLI) and a linear regression model (least square method) was applied, constraining the model to pass at the origin (i.e., the condition in which there is no tracer, the CNR output should be close to zero). Statistical analysis was performed with IBM SPSS® Statistics Version 26 (IBM, Armonk, USA).

1 **Results**

2 Preclinical-Setup: Mouse model

3 Our in vitro assay with ^{18}F -PSMA demonstrated activity levels in Eppendorf-tubes up to
4 5.46 kBq/ml for CLI and 1.60 kBq/ml for FAR-CLI (Supplementary Figure 2). Linear regression
5 between AC and CNR revealed r-square values of 0.91 and 0.85 (both $p < 0.0001$).

6 In microPET/CT the reconstructed median AC two hours after tracer administration was
7 651.72 kBq/ml, 608.56 kBq/ml, and 52.99 kBq/ml, for the left kidney, right kidney and PC-tissue,
8 respectively. Linear regression between CLI CNR and the decay corrected PET AC of the 2 h pi
9 microPET/CT demonstrated r-squares of 0.92 ($p < 0.0001$) and 0.62 ($p < 0.0001$) for the excised
10 organs and whole mouse, respectively (Figure 2).

11 During examination of the whole mouse, visualization of the subcutaneous PC-tissue was
12 not possible in CLI in either of the 5 cases. In FAR-CLI 3 cases showed a weak signal with a
13 minimum AC of 22.16 kBq/ml at a CNR of 7.07. Regarding the examination of excised PC-tissue,
14 in CLI no signal was detectable with a maximum AC of up to 15 kBq/ml. In contrast, ^{18}F -PSMA
15 uptake could be visualized by FAR-CLI in all 5 PC samples with a lowest detected AC and CNR
16 of 7.25 kBq/ml and 5.48, respectively (Figure 3). Despite the different detection threshold, there
17 was no statistical difference between both FAR-CLI and CLI ($p < 0.09$) and least square linear
18 regression shows good agreement between both modalities ($r\text{-square} = 0.75$; $p = 0.05$). Direct
19 examination of high ACs revealed a contiguous uptake region of the kidneys and PC tissue in
20 FAR-CLI. The signal from the PC tumors could be reliably visualized in the single examination
21 (Supplementary Figure 3). Subsequently, the specimens were placed further apart in the
22 subsequent measurements.

23 At time of imaging there was no significant difference in tracer AC between CLI and FAR-
24 CLI but a significant increase in CNR of visible foci (Supplementary Table 1). Correlation analysis
25 showed a strong correlation between a higher AC of the excised kidneys and PC-tissue with a
26 higher CNR, Spearman's $\rho = 0.783$, $p < 0.001$ for CLI and Spearman's $\rho = 0.712$, $p < 0.001$ for
27 FAR-CLI. Examination of the whole mouse also showed a strong correlation for CLI with
28 Spearman's $\rho = 0.559$, $p < 0.001$ and FAR-CLI with Spearman's $\rho = 0.379$, $p = 0.01$.

29

30 Clinical-Setup: Radical prostatectomy

31 In total 7 patients were included in this feasibility study, among those 6 with a high-risk of
32 progression according to NCCN-guidelines(31). Imaging and patient characteristics are displayed
33 in Table 1.

1 CLI detected a median of 2 lesions on the prostate surface, one of these always at the
2 bladder neck, with a median CNR of 33.96 (Table 2). In terms of CNR and number of lesions
3 detected, there was a significant reduction using FAR-CLI ($p=0.02$), at comparable AC levels. Two
4 patients showed PRMs after histopathological evaluation. The PRMs consisted once of an
5 International Society of Urological Pathology Gleason Grading Group (ISUP-GGG) 4 with a
6 diameter of 2 mm. Both CLI and FAR-CLI showed no signal in the corresponding localisation. The
7 second PRM with ISUP-GGG 1 and a diameter of 1 mm also showed no corresponding image
8 morphological correlate in CLI and FAR-CLI. The PRM is histopathologically located apically
9 dorsal right. CLI and FAR-CLI showed a suspicious signal apical lateral right (Supplementary
10 Figure 4).

11 After incision over the MRI-informed index lesion, no luminescence in CLI with a median
12 CNR of 0.26 was detectable. The mean gain in sensitivity of FAR-CLI in comparison to CLI was
13 evaluated for Eppendorf tubes, by calculating the fold increase in radiance normalised for AC.
14 FAR-CLI showed an approximately 2.1-fold radiance enhancement (Supplementary Figure 5).
15 Median AC at time of incision was 3.06 kBq/ml. In contrast, a suspicious luminescence of PC was
16 detectable in 6 of 7 patients in FAR-CLI (Figure 4). The AC of the one missed index lesion was
17 1.85 kBq/ml, resulting in a detection limit of at least 2.06 kBq/ml with a median CNR of 8.78. Direct
18 anatomical correlation is challenging due to the scintillator overlay.

1 Discussion

2 In mice with subcutaneous PSMA-avid PC, different levels of AC were evaluated in terms
3 of visualization. Due to the different tracer uptake in kidneys and PC-tissue, it was possible to
4 generate a broad spectrum of signals over time. Previously, Olde Heuvel et al. described a
5 detection limit of 3.42 kBq/ml for ^{18}F -CLI in vitro (32). Our in vitro assay demonstrated similar
6 findings with a detection limit in Eppendorf-tubes of 5.46 kBq/ml for CLI and 1.60 kBq/ml for FAR-
7 CLI. Such a radiance enhancement was also reported by Pratt and colleagues, who evaluated
8 nanoparticles in the presence of beta emitters (33). In contrast, no significant CLI signal from PC-
9 tissue up to 15 kBq/ml was observed in our mouse model. The discrepancies between in-vitro and
10 mouse measurements can be explained by the absorption (for example by hemoglobin) and
11 scattering in biological tissues which severely limits sensitivity (34). Based on our study design
12 with preoperative tracer injection and an estimated time from injection to prostate examination of
13 approximately 5 hours, AC above 15 kBq/ml is not expected. In contrast to CLI, FAR-CLI
14 visualized PC tissue up to an activity of 7.25 kBq/ml. A clear discrimination was possible with a
15 median CNR of 5.48, so that FAR-CLI seems to be a promising modality for low AC levels. We
16 were able to show that subcutaneous (at < 1 mm depth) PC tumors could be visualized down to
17 the lowest measured AC of 23.02 kBq/ml in FAR-CLI.

18 Next, we tested FAR-CLI in men undergoing RP. This first-in-man study investigated the
19 feasibility to assess tumor margin status and to evaluate minimum detection limits.

20 After incision there was no increased signal in CLI visible. CLI using a ^{18}F -PSMA did not
21 provide any useful signals, only luminescence artifacts. In contrast, with the aid of the flexible
22 scintillator, FAR-CLI detected cancer foci. The minimum detectable AC here was 2.06 kBq/ml with
23 a CNR of 10.84. On this basis, a good detection of PRMs should be assumed. However, the use
24 of FAR-CLI for PRM assessment is challenging. PRM were found in 2 patients. In one patient,
25 histology demonstrated a 2 mm positive margin with an ISUP-GGG 4 at the left seminal vesicle
26 plateau, but even using FAR-CLI no signal in this area was visible. The second PRM with an ISUP-
27 GGG of 1 and a length of 1 mm also showed no corresponding correlate in FAR-CLI.

28 Jurrius et al. also investigated the use of a flexible autoradiography imaging to assess
29 resection margins. In the context of breast-conserving surgery with ^{18}F -FDG, an overall accuracy
30 of 80.5% was shown, with a sensitivity of 46.2%. Although a direct comparison between breast
31 and prostate cancer is difficult, our results do not show the same benefit for FAR-CLI. On the one
32 hand, this may be due to tumor biology, on the other hand, it may be related to the study design.
33 A major difference is the timing between tracer injection and measurement of CLI or FAR-CLI

1 activity. In our study, measurements were taken about 2 hours later compared to the work of
2 Jurrius et al (23).

3 In principle, every radioguided-surgery technique requires high contrast-to-noise ratio, high
4 sensitivity and user friendliness, in order to provide a net benefit for patients and surgeons in
5 routine care. CLI is able to provide a very good surface contrast, however, as it is shown in this
6 report, insufficient sensitivity at very low activities, mainly due to tissue light absorption. On the
7 other hand, FAR-CLI, is able to compensate the lack of sensitivity by increasing the net light output
8 per emitted beta particle, but it leads to a lower spatial resolution of imaged foci, making difficult
9 the discrimination of closely located uptake regions. Furthermore, there is a high sensitivity of the
10 CLI/FAR-CLI to ambient light, so that measurements can only be made in a light-tight chamber.
11 This must be considered for further implementation of the system. A possible improvement to the
12 presented method could be achieved by topical application of nanoparticles. Pratt et al described
13 the advantages of Gd_2O_3 and Eu_2O_3 , which showed the largest enhancement in radiance. The
14 combination of Gd_2O_3 and Eu_2O_3 with ^{68}Ga and ^{18}F , respectively, produced distinct visible emission
15 peaks (33).

16 Additional limitations of our manuscript deserve further discussion. In our study setting,
17 ^{18}F -PSMA represents a suboptimal tracer due to very low activity in the context of RP. Although
18 the half-life is prolonged in contrast to other tracers, the emitted energy is lower. Adjustment of
19 the current workflow is necessary with respect to higher activity levels at the time of RP. This will
20 require future optimizations in dosing and timing. However, radiation exposure for medical
21 personnel and patients must be considered as well as possible negative effects on specificity. The
22 fact that in most of the patients after incision a signal was detected in FAR-CLI demonstrated
23 feasibility of ^{18}F -PSMA-FAR-CLI. In case of suspicious findings, CLI could subsequently be used
24 for surface assessment. The extent to which this can be applied clinically remains to be
25 investigated in future studies. The flexible scintillation film is semi-opaque and thus obscures the
26 white light reference image of the sample, which presents a challenge for accurate correlation of
27 the FAR-CLI signal with the exact anatomical location on the sample.

28 **Conclusion**

29 The detection of PC by using ^{18}F -PSMA-FAR-CLI is possible - even at low activity levels down to
30 2.06 kBq/ml. However, anatomical correlation is difficult and detection of PRM failed. ^{18}F -PSMA-
31 CLI had no value in this setup.

32

1 **Disclosure statement**

2 **CK:** reports consulting fees Apogepha, research funding Advanced Accelerator Applications
3 (Novartis).

4 **ST** reports personal and travel fees from Ipsen, Eisai, Bayer, Janssen, Novartis, Bristol-Myers-
5 Squibb and BrachySolutions; research funding from Ipsen

6 **JPR** reports personal and travel fees from Invivo Uronav, Bender Group, Beckelmann and
7 Partners and Saegeling Medizintechnik; and research funding from Advanced Accelerator
8 Applications and Novartis.

9 **KH** reports personal fees from Bayer, Sofie Biosciences, SIRTEX, Adacap, Curium, Endocyte and
10 BTG

11 **WPF** reports fees from SOFIE Bioscience (research funding), Janssen (consultant, speakers
12 bureau), Calyx (consultant), Bayer (consultant, speakers bureau, research funding), and Parexel
13 (image review) outside of the submitted work.

14 **BAH** reports personal fees from ABX, Bayer, LightPoint Medical Inc., Janssen R&D, Bristol-Myers-
15 Squibb and Astellas; research funding from Profound Medical, German Cancer Aid, German
16 Research Foundation, Janssen R&D, Bristol-Myers-Squibb, MSD, Pfizer and Astellas; and travel
17 fees from AstraZeneca, Janssen R&D and Astellas.

18
19 This work was supported by the “Deutsche Forschungsgemeinschaft - DFG” (Project number:
20 Projekt HA 5160/5-1). The other authors declare that no relevant conflicts of interest that may
21 directly or indirectly influence the content of the manuscript submitted exist.

22

1 **Key-Points**

2 *Question:*

3 Are Cerenkov Luminescence (CLI) and Flexible Autoradiography Imaging (FAR-CLI) useful
4 for displaying prostate cancer cells close to or at the surface of prostatectomy specimen?
5

6 *Pertinent findings:*

7 In this feasibility study 7 patients undergoing radical prostatectomy with a ¹⁸F-PSMA-
8 PET/CT scan on the same day were analysed for suspicious intensity levels. FAR-CLI, in contrast
9 to CLI, was able to clearly highlight prostate cancer cells from surrounding tissue after incision.
10 However, detection of prostate cancer in positive resection margins was not possible by either
11 modality.
12

13 *Implication for patient care:*

14 ¹⁸F-CLI has no value for the detection of resection margins in a pre-operative ¹⁸F-PSMA
15 administration protocol. ¹⁸F-FAR-CLI is possible, but without meaningful clinical benefit.
16

1 **References**

- 2
- 3 **1.** EAU Guidelines. Edn. presented at the EAU Annual Congress Amsterdam 2022. .
- 4
- 5 **2.** Iczkowski KA, Lucia MS. Frequency of positive surgical margin at prostatectomy and its
- 6 effect on patient outcome. *Prostate Cancer*. 2011;2011:673021.
- 7
- 8 **3.** Yossepowitch O, Briganti A, Eastham JA, et al. Positive surgical margins after radical
- 9 prostatectomy: a systematic review and contemporary update. *Eur Urol*. 2014;65:303-313.
- 10
- 11 **4.** Schlomm T, Tennstedt P, Huxhold C, et al. Neurovascular structure-adjacent frozen-
- 12 section examination (NeuroSAFE) increases nerve-sparing frequency and reduces positive
- 13 surgical margins in open and robot-assisted laparoscopic radical prostatectomy: experience
- 14 after 11,069 consecutive patients. *Eur Urol*. 2012;62:333-340.
- 15
- 16 **5.** Nyarangi-Dix J, Wiesenfarth M, Bonekamp D, et al. Combined Clinical Parameters and
- 17 Multiparametric Magnetic Resonance Imaging for the Prediction of Extraprostatic Disease-A Risk
- 18 Model for Patient-tailored Risk Stratification When Planning Radical Prostatectomy. *Eur Urol*
- 19 *Focus*. 2018.
- 20
- 21 **6.** Petralia G, Musi G, Padhani AR, et al. Robot-assisted radical prostatectomy:
- 22 Multiparametric MR imaging-directed intraoperative frozen-section analysis to reduce the rate
- 23 of positive surgical margins. *Radiology*. 2015;274:434-444.
- 24
- 25 **7.** Collamati F, van Oosterom MN, Hadaschik BA, Fragoso Costa P, Darr C. Beta radioguided
- 26 surgery: towards routine implementation? *Q J Nucl Med Mol Imaging*. 2021;65:229-243.
- 27
- 28 **8.** Olde Heuvel J, de Wit-van der Veen BJ, Huizing DMV, et al. State-of-the-art
- 29 Intraoperative Imaging Technologies for Prostate Margin Assessment: A Systematic Review. *Eur*
- 30 *Urol Focus*. 2021;7:733-741.
- 31
- 32 **9.** Meershoek P, van Oosterom MN, Simon H, et al. Robot-assisted laparoscopic surgery
- 33 using DROP-IN radioguidance: first-in-human translation. *European journal of nuclear medicine*
- 34 *and molecular imaging*. 2019;46:49-53.
- 35
- 36 **10.** Maurer T, Robu S, Schottelius M, et al. (99m)Technetium-based Prostate-specific
- 37 Membrane Antigen-radioguided Surgery in Recurrent Prostate Cancer. *Eur Urol*. 2019;75:659-
- 38 666.
- 39
- 40 **11.** Maurer T, Graefen M, van der Poel H, et al. Prostate-Specific Membrane Antigen-Guided
- 41 Surgery. *J Nucl Med*. 2020;61:6-12.
- 42

- 1 **12.** Knipper S, Mehdi Irai M, Simon R, et al. Cohort Study of Oligorecurrent Prostate Cancer
2 Patients: Oncological Outcomes of Patients Treated with Salvage Lymph Node Dissection via
3 Prostate-specific Membrane Antigen-radioguided Surgery. *Eur Urol.* 2022.
4
- 5 **13.** Koehler D, Sauer M, Klutmann S, et al. Feasibility of (99m)Tc-MIP-1404 for SPECT/CT
6 imaging and subsequent PSMA-radioguided surgery in early biochemical recurrent prostate
7 cancer: a case series of 9 patients. *J Nucl Med.* 2022.
8
- 9 **14.** Collamati F, van Oosterom MN, De Simoni M, et al. A DROP-IN beta probe for robot-
10 assisted 68Ga-PSMA radioguided surgery: first ex vivo technology evaluation using prostate
11 cancer specimens. *EJNMMI research.* 2020;10:1-10.
12
- 13 **15.** Debacker JM, Schelfhout V, Brochez L, et al. High-Resolution (18)F-FDG PET/CT for
14 Assessing Three-Dimensional Intraoperative Margins Status in Malignancies of the Head and
15 Neck, a Proof-of-Concept. *J Clin Med.* 2021;10.
16
- 17 **16.** Grootendorst MR, Cariati M, Pinder SE, et al. Intraoperative Assessment of Tumor
18 Resection Margins in Breast-Conserving Surgery Using (18)F-FDG Cerenkov Luminescence
19 Imaging: A First-in-Human Feasibility Study. *J Nucl Med.* 2017;58:891-898.
20
- 21 **17.** Chin PT, Welling MM, Meskers SC, Valdes Olmos RA, Tanke H, van Leeuwen FW. Optical
22 imaging as an expansion of nuclear medicine: Cerenkov-based luminescence vs fluorescence-
23 based luminescence. *Eur J Nucl Med Mol Imaging.* 2013;40:1283-1291.
24
- 25 **18.** Darr C, Harke N, Radtke JP, et al. Intraoperative (68)Gallium-PSMA Cerenkov
26 Luminescence Imaging for surgical margins in radical prostatectomy - a feasibility study. *J Nucl*
27 *Med.* 2020.
28
- 29 **19.** Olde Heuvel J, de Wit-van der Veen BJ, van der Poel HG, et al. (68)Ga-PSMA Cerenkov
30 luminescence imaging in primary prostate cancer: first-in-man series. *Eur J Nucl Med Mol*
31 *Imaging.* 2020.
32
- 33 **20.** Darr C, Fragoso Costa P, Kesch C, et al. Prostate specific membrane antigen (PSMA)-radio
34 guided surgery using Cerenkov luminescence imaging—utilization of a short-pass filter to reduce
35 technical pitfalls. *Translational Andrology and Urology.* 2021.
36
- 37 **21.** Gill RK, Mitchell GS, Cherry SR. Computed Cerenkov luminescence yields for
38 radionuclides used in biology and medicine. *Phys Med Biol.* 2015;60:4263-4280.
39
- 40 **22.** Vyas KN, Grootendorst M, Mertzaniidou T, et al. *Flexible scintillator autoradiography for*
41 *tumor margin inspection using 18F-FDG.* Vol 10478: SPIE; 2018.
42
- 43 **23.** Jurrius P, Grootendorst MR, Krotewicz M, et al. Intraoperative [(18)F]FDG flexible
44 autoradiography for tumour margin assessment in breast-conserving surgery: a first-in-human
45 multicentre feasibility study. *EJNMMI Res.* 2021;11:28.

- 1
2 **24.** Annual Congress of the European Association of Nuclear Medicine October 13 – 17, 2018
3 Düsseldorf, Germany. *European Journal of Nuclear Medicine and Molecular Imaging*. 2018;45:1-
4 844.
5
6 **25.** Lückerath K, Stuparu AD, Wei L, et al. Detection Threshold and Reproducibility of (68)Ga-
7 PSMA11 PET/CT in a Mouse Model of Prostate Cancer. *J Nucl Med*. 2018;59:1392-1397.
8
9 **26.** Olde Heuvel J, de Wit - van der Veen L, Tuch D, Vyas K, Stokkel M, Slump C. Performance
10 evaluation of Cerenkov Luminescence Imaging: A comparison of 68Ga with 18F. *Journal of*
11 *Nuclear Medicine*. 2018;59:365.
12
13 **27.** Fendler WP, Eiber M, Beheshti M, et al. (68)Ga-PSMA PET/CT: Joint EANM and SNMMI
14 procedure guideline for prostate cancer imaging: version 1.0. *Eur J Nucl Med Mol Imaging*.
15 2017;44:1014-1024.
16
17 **28.** Fragoso Costa P, Fendler WP, Herrmann K, et al. Radiation Protection and Occupational
18 Exposure on [(68)Ga]Ga-PSMA-11 based Cerenkov Luminescence Imaging Procedures in robot
19 assisted Prostatectomy. *J Nucl Med*. 2021.
20
21 **29.** Ciarrocchi E, Vanhove C, Descamps B, De Lombaerde S, Vandenberghe S, Belcari N.
22 Performance evaluation of the LightPath imaging system for intra-operative Cerenkov
23 luminescence imaging. *Phys Med*. 2018;52:122-128.
24
25 **30.** Bright DS, Newbury DE, Steel EB. Visibility of objects in computer simulations of noisy
26 micrographs. *Journal of microscopy*. 1998;189:25-42.
27
28 **31.** National Comprehensive Cancer Network. Prostate Cancer (Version 3.2022).
29 https://www.nccn.org/professionals/physician_gls/pdf/prostate.pdf. Accessed February 06,
30 2022.
31
32 **32.** Olde Heuvel J, de Wit-van der Veen BJ, Vyas KN, et al. Performance evaluation of
33 Cerenkov luminescence imaging: a comparison of (68)Ga with (18)F. *EJNMMI Phys*. 2019;6:17.
34
35 **33.** Pratt EC, Shaffer TM, Zhang Q, Drain CM, Grimm J. Nanoparticles as multimodal photon
36 transducers of ionizing radiation. *Nat Nanotechnol*. 2018;13:418-426.
37
38 **34.** Ciarrocchi E, Belcari N. Cerenkov luminescence imaging: physics principles and potential
39 applications in biomedical sciences. *EJNMMI Phys*. 2017;4:14.
40

1 **Tables and Figures**

2

3 **Table 1**

Imaging characteristics	
Activity injected in MBq Median (IQR)	312 (280; 332)
Tracer activity at PET/CT in kBq/ml Median (IQR)	17.71 (12.46; 34)
Activity at CLI in kBq/ml Median (IQR)	3.54 (2.57; 6.91)
Time from injection to CLI/FAR-CLI in min Median (IQR)	329 (308; 333)
Contrast-to-noise ratio CLI: median (IQR) FAR-CLI: median (IQR)	0.26 (0; 1.5) 9.13 (4.13; 19.23)
Patient characteristics	
Age in years Median (IQR)	65.14 (63, 67)
Initial PSA in ng/ml Median (IQR)	11 (5.1, 22)
NCCN-risk at biopsy High-risk, n (%) Intermediate-risk, n (%)	6 (86%) 1 (14%)
NCCN-risk score at final histopathology High-risk, n (%) Intermediate-risk, n (%)	5 (71%) 2 (29%)
Resection-Status R1-Resection R0-Resection	2 (29%) 5 (71%)

4 Nuclear medicine and patient characteristics. Values are given as median and interquartile range
5 or absolute numbers and percent. FAR: Flexible Autoradiography, CLI: Cerenkov Luminescence
6 Imaging, IQR: Interquartile range, NCCN: National Comprehensive Cancer Network, PSA:
7 prostate-specific antigen

8

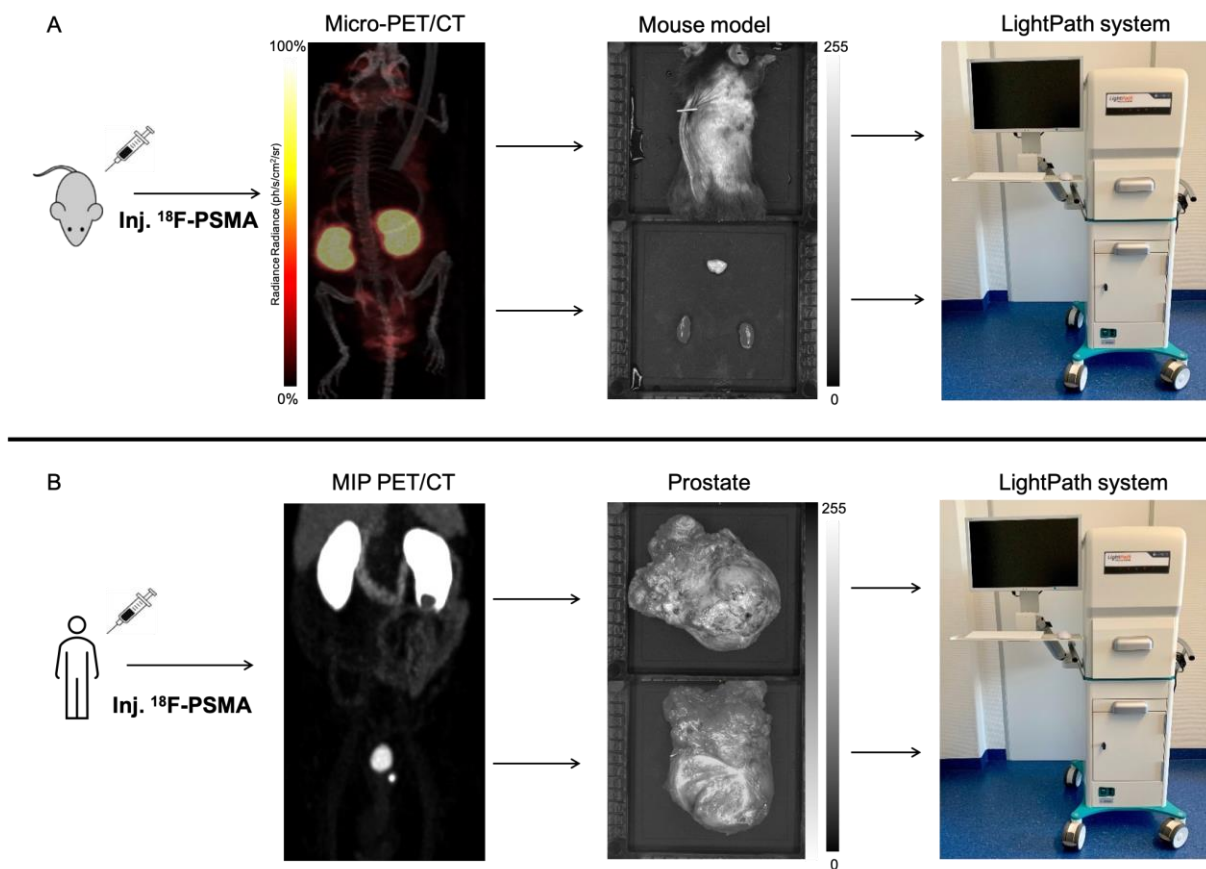
1 **Table 2**

2

Intact prostate specimen (n=7)			
	CLI	FAR-CLI	p-value
Activity in kBq/ml Median (IQR)	3.53 (2.57, 6.91)	3.95 (2.16, 7.22)	n.s.
CNR Median (IQR)	33.96 (15.71, 43.29)	6.13 (4.07, 21.43)	0.02
Lesions Median (IQR)	2 (1, 2)	1 (0.5, 1)	0.02
Incised prostate specimen (n=7)			
	CLI	FAR-CLI	p-value
Activity in kBq/ml Median (IQR)	3.06 (1.98, 5.98)	2.8 (2.06, 5.72)	n.s.
CNR Median (IQR)	0.26 (0, 1.5)	9.53 (4.13, 19.23)	0.002

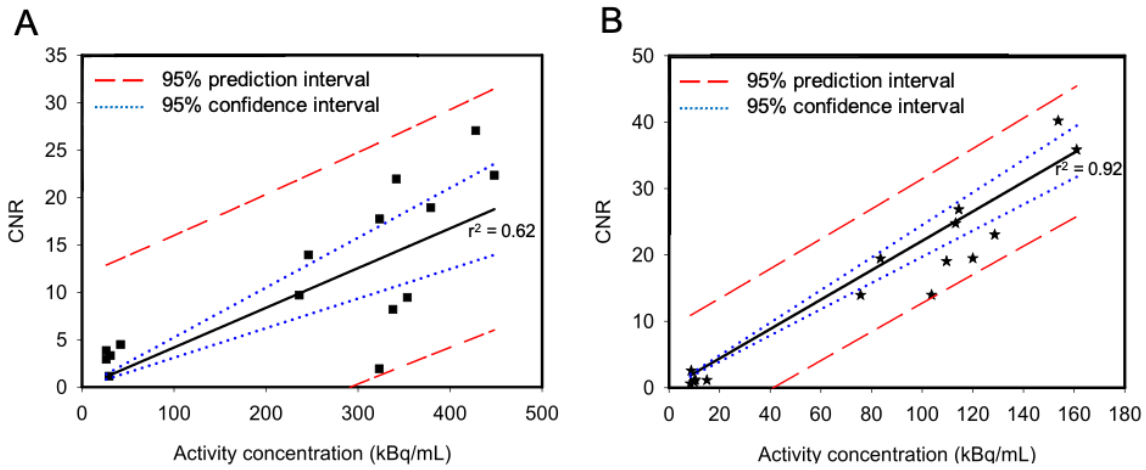
3 Cerenkov Luminescence and Autoradiography Imaging measurements of the prostatectomy
 4 specimen with the corresponding activity levels. Measured intensities are stated as contrast-to-
 5 noise ratio. All data are given in median and interquartile range. Significance set at $p < 0.05$. FAR:
 6 Flexible Autoradiography, CLI: Cerenkov Luminescence Imaging, CNR: Contrast-to-noise-ratio,
 7 IQR: Interquartile range, n.s.: not significant
 8

1
2 **Figure 1**



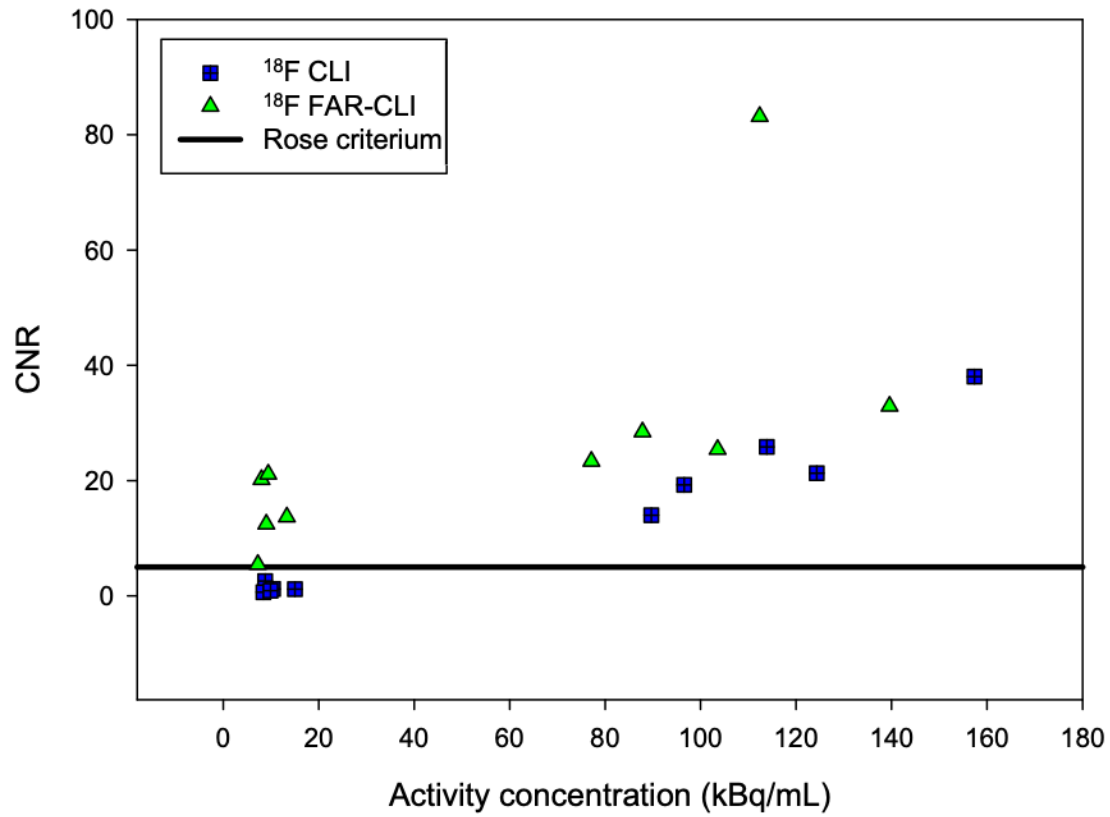
3
4 Study design. A: Injection of ^{18}F -PSMA into tumor-bearing mice. 2 hours afterwards, microPET/CT
5 was performed. Next, Cerenkov Luminescence Imaging (CLI) and Flexible Autoradiography (FAR)
6 of the whole mouse were acquired followed by analysis of the excised kidneys and prostate
7 carcinoma tissue.
8 B: In a second approach, the examination of the prostate specimen in patients undergoing radical
9 prostatectomy was performed, with direct preoperative ^{18}F -PSMA PET/CT. Removal of the
10 prostate was followed by immediate examination of the intact prostate specimen and the target
11 lesion (after incision) by CLI and FAR.
12

1 **Figure 2**



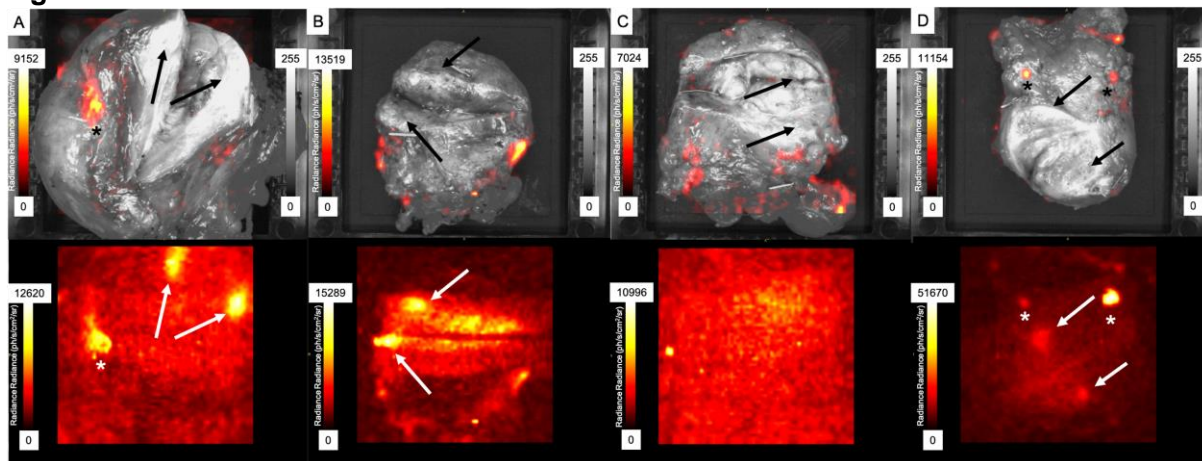
2
3 Linear regression of preclinical Cerenkov Luminescence Imaging (CLI) with the standardized
4 imaging protocol. Contrast-to-noise ratio is plotted against microPET/CT activity concentration.
5 Figure A shows the PET vs. whole mouse CLI comparison. Figure B shows PET vs. excised
6 kidneys and prostate carcinoma tissue comparison.
7

1 **Figure 3**



2
3 Visual detectability of the excised kidneys and prostate cancer tissue. Contrast-to-noise ratio is
4 plotted against microPET/CT activity concentration. The highest AC region corresponds to signals
5 from the kidneys, while the lowest cluster refers to prostate cancer signals. Foci with a CNR ≥ 5
6 were considered detectable (Rose criterium).
7

1 **Figure 4**



2
3 Gray-scale photographic images overlaid with Cerenkov signals (CLI, A-D top) and
4 Autoradiography-Imaging (FAR-CLI, A-D bottom) of incised prostate specimens. In CLI no
5 Hotspots in the prostate cancer lesion was observed (A-D top, black arrow). Hotspots in the FAR-
6 CLI are indicated by white arrows. The corresponding area in CLI is marked with black arrows.
7 Artificial signals in CLI are marked with a black * and the correlating FAR-CLI-signals are marked
8 with a white *. Histopathology proved the absence of prostate cancer (PC) at the surface. A and
9 B (bottom) show a good signal in FAR-CLI with a contrast-to-noise ratio (CNR) of 9.13 and 23.03.
10 In C (bottom), no increased signal was detectable in PC with an activity of 1.85 kBq/ml and a
11 corresponding CNR of 3.69. In D (bottom) increased signals with a CNR of 10.84 at an activity of
12 2.06 kBq/ml was visible.

1 **Supplementary Material**

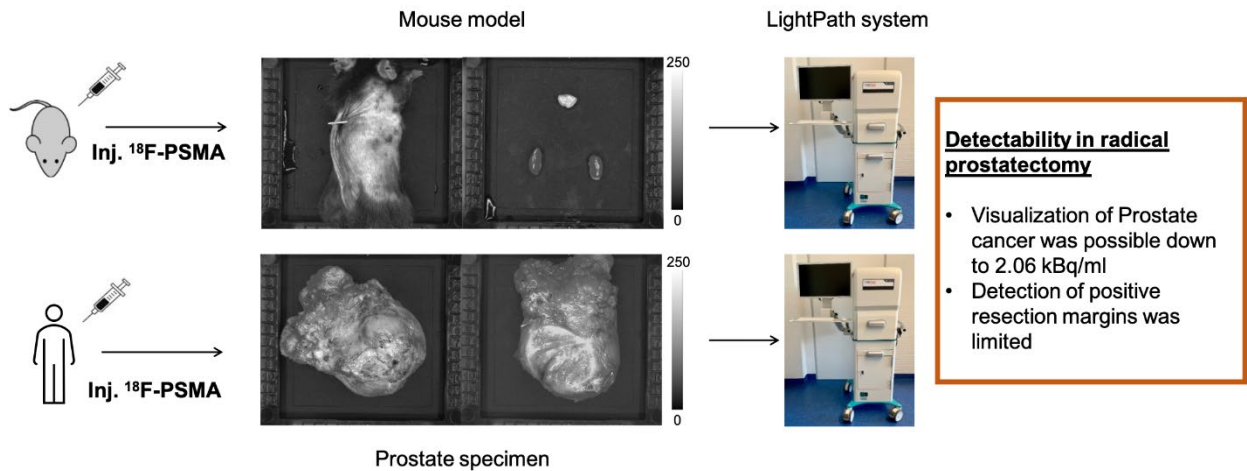
2

3 **Supplementary Table 1**

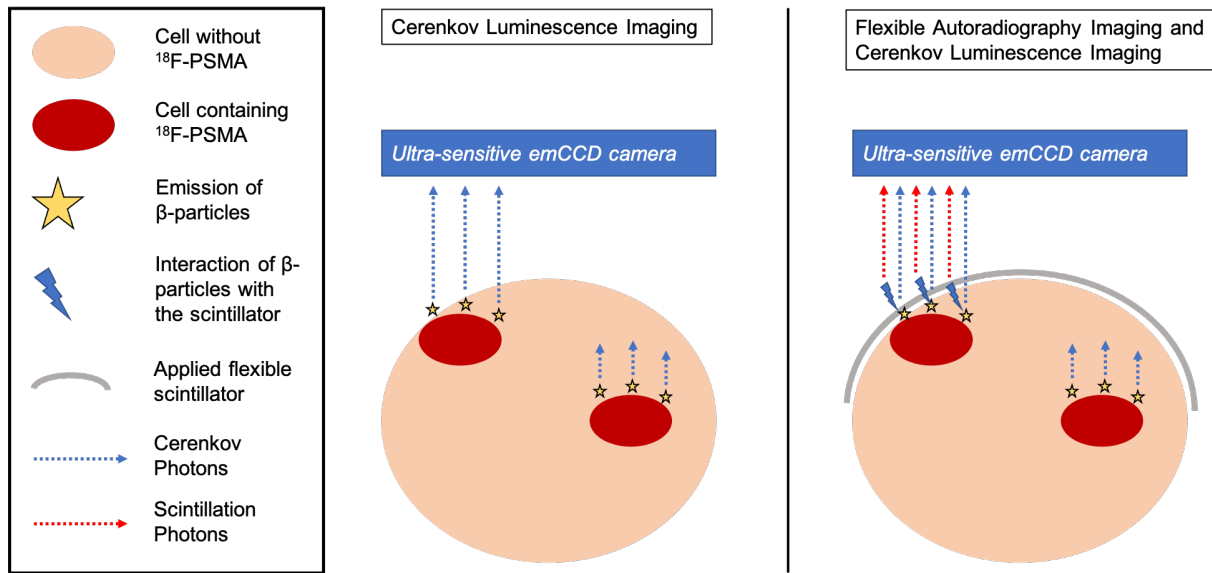
Mouse model			
Kidneys (n=10)	CLI	FAR-CLI	p-value
Activity in kBq/ml Median (IQR)	339.58 (303.67; 391.12)	296.38 (268.97, 361.94)	n.s.
CNR Median (IQR)	15.85 (9.15; 22.06)	16.12 (8.71, 22.78)	n.s.
Prostate cancer (n=5)	CLI	FAR-CLI	
Activity in kBq/ml Median (IQR)	29.23 (26.26, 36.21)	26.92 (22.85, 33.45)	n.s.
CNR Median (IQR)	3.33 (2.05, 4.18)	4.1 (3.03, 12.03)	n.s.
Kidneys / Prostate cancer			
Kidneys (n=10)	CLI	FAR-CLI	p-value
Activity in kBq/ml Median (IQR)	113.85 (98.65, 134.93)	103.56 (85.82, 121.3)	n.s.
CNR Median (IQR)	21.29 (17.8, 29.12)	28.68 (26.32, 47.25)	0.04
Prostate cancer (n=5)	CLI	FAR-CLI	
Activity in kBq/ml Median (IQR)	9.92 (8.61, 12.71)	9.03 (7.63, 11.36)	n.s.
CNR Median (IQR)	1.16 (0.77, 1.89)	13.7 (8.97, 20.65)	0.009

4 Cerenkov luminescence and flexible autoradiography imaging measurements of the mouse model
5 and the kidneys / prostate cancer tissue with the corresponding activity levels. Measured
6 intensities are stated as contrast to noise ratio (CNR). All data are given as median and
7 interquartile range. Significance was set at $p < 0.05$. FAR: Flexible Autoradiography, CLI: Cerenkov
8 Luminescence Imaging, CNR: Contrast-to-noise-ratio, IQR: Interquartile range, n.s.: not significant
9

Graphical abstract

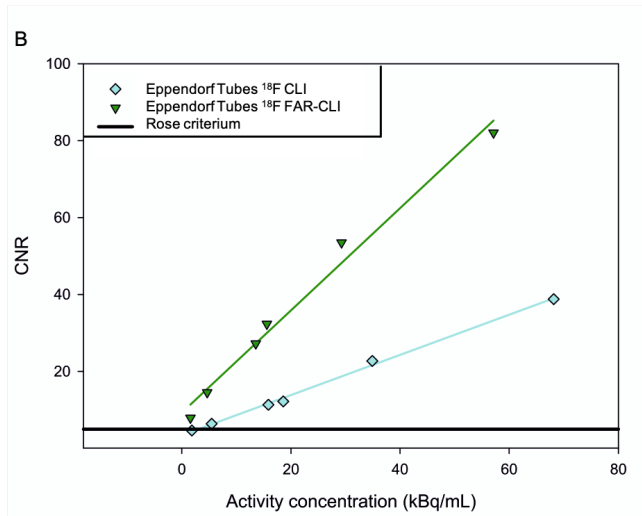
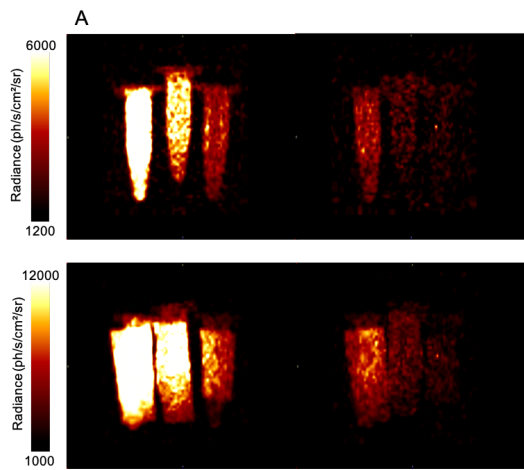


1 **Supplementary Figure 1**



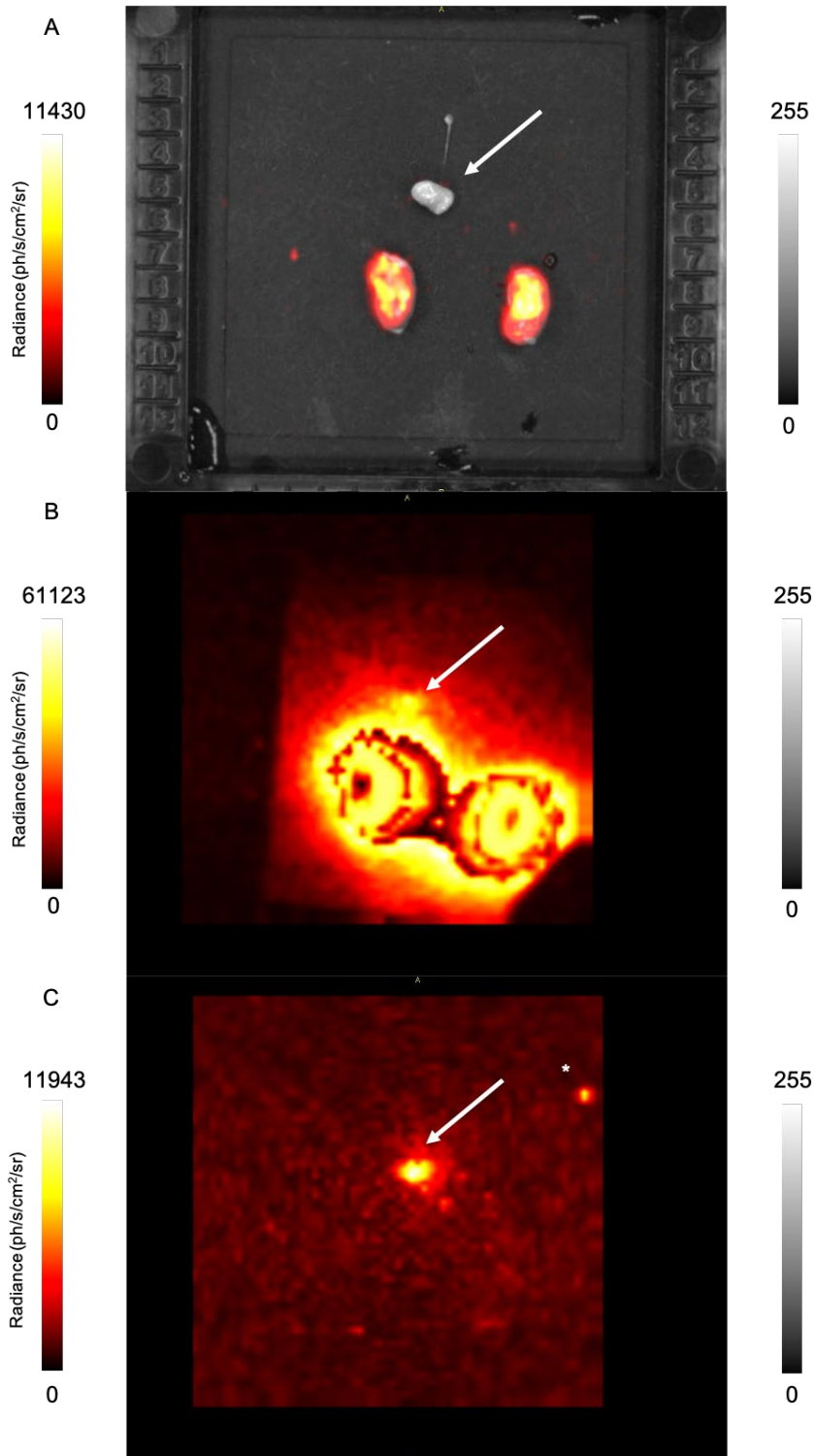
2
 3 Schematic representation of Cerenkov Luminescence Imaging on the left and Flexible
 4 Autoradiography and Cerenkov Luminescence Imaging on the right using a flexible scintillating
 5 film. Tumor cells binding ^{18}F -PSMA emit β -particles, which in turn emit Cerenkov optical
 6 photons or which are converted to scintillation photons by the flexible scintillator. As β -particles
 7 travel a limited distance in tissue, ^{18}F -PSMA containing cells are detected only near the surface.
 8 The photons (Cerenkov photons and scintillation photons) are measured by an ultra-sensitive
 9 emCCD camera.

1 Supplementary Figure 2



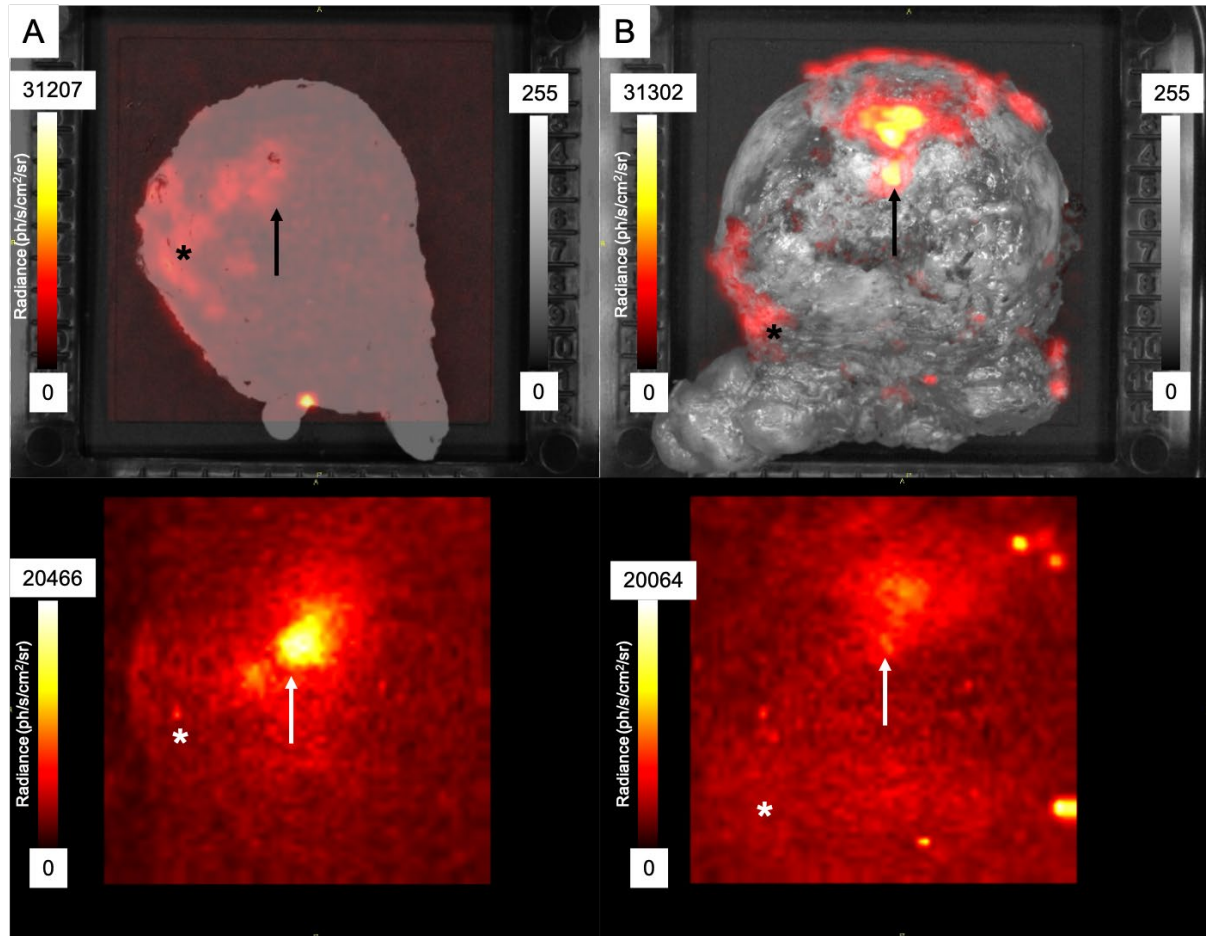
2
3 CLI (panel A top row) and FAR-CLI (panel A bottom row) radiance (photons/s/cm²/sr) of ¹⁸F
4 solutions in Eppendorf tubes. Through dilution series (using distilled water), activity concentrations
5 (AC) between 66.2 - 1.9 kBq/ml for CLI and 57.13 - 1.6 kBq/ml for FAR-CLI were examined. A
6 illustrates the 3 highest ACs on the left, from outside to inside and the lowest 3 ACs on the right,
7 from inside to outside; see panel B. Linearity and minimum detectable activity concentration are
8 shown in panel B.

1 **Supplementary Figure 3**



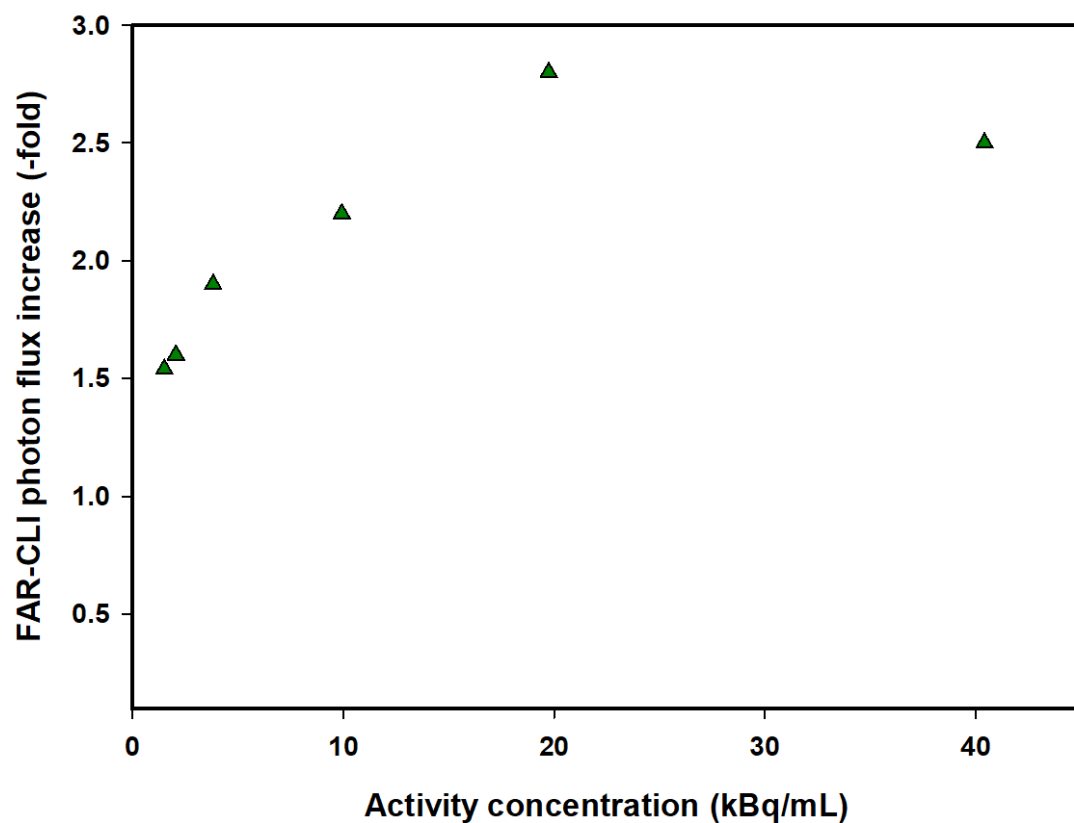
2
3 Gray-scale photographic images overlaid with CLI signals of the two mouse kidneys at the bottom
4 and prostate cancer (PC) tissue at the top (A). In FAR-CLI (B) the PC signal cannot be clearly
5 delineated (arrow) due to the strong radiation of the kidneys; thus, a separate image was taken
6 only from PC. FAR-CLI showed a good signal of PC with a contrast-to-noise ratio of 20.16 and an
7 activity of 7.85 kBq/ml; the asterisk marks an artificial signal (C).

1 **Supplementary Figure 4**



2
3 Gray-scale photographic images overlaid with Cerenkov signals (CLI, A+B top) and Flexible
4 Autoradiography (FAR-CLI, A+B bottom) of two intact prostate specimens with histopathological
5 proven positive resection margins (PRM). The area of the PRM is marked with a black asterisk *
6 for CLI and a white asterisk * for FAR-CLI. Hotspots in FAR-CLI are indicated by white arrows,
7 with the corresponding area in CLI indicated by black arrows. In images A, histopathology
8 showed a PRM apically dorsal left, without corresponding photon signals. In images B,
9 histopathology showed a PRM at the left seminal vesicle plateau, but a corresponding image
10 signal could only be derived at the ventral prostate surface.

1 **Supplementary Figure 5**



- 2
3 Radiance enhancement of FAR-CLI relatively to CLI in Eppendorf tubes filled with ^{18}F . Here the
4 background corrected radiance levels were normalised to the activity concentration, decay
5 corrected to the time-point of measurement.